Turbulence in the TORE SUPRA Tokamak: Measurements and Validation of Nonlinear Simulations

A. Casati,[1,*] T. Gerbaud,[1,2] P. Hennequin,[2] C. Bourdelle,[1] J. Candy,[3] F. Clairet,[1] X. Garbet,[1] V. Grandgirard,[1] Ö. D. Gürcan,[2] S. Heuraux,[4] G. T. Hoang,[1] C. Honoré,[2] F. Imbeaux,[1] R. Sabot,[1] Y. Sarazin,[1] L. Vermare,[2] and R. E. Waltz[3]

[1]*CEA, IRFM, F-13108 Saint-Paul-lez-Durance, France*
[2]*Laboratoire de Physique des Plasmas, CNRS-École Polytechnique, 91128 Palaiseau Cedex, France*
[3]*General Atomics, P.O. Box 85608, San Diego, California 92186-5608, USA*
[4]*IJL, CNRS Nancy-Université, 54052 Nancy Cedex, France*

(Received 18 February 2009; published 24 April 2009)

Turbulence measurements in TORE SUPRA tokamak plasmas have been quantitatively compared to predictions by nonlinear gyrokinetic simulations. For the first time, numerical results simultaneously match within experimental uncertainty (a) the magnitude of effective heat diffusivity, (b) rms values of density fluctuations, and (c) wave-number spectra in both the directions perpendicular to the magnetic field. Moreover, the nonlinear simulations help to revise as an instrumental effect the apparent experimental evidence of strong turbulence anisotropy at spatial scales of the order of ion-sound Larmor radius.

DOI: 10.1103/PhysRevLett.102.165005 PACS numbers: 52.55.Dy, 52.35.Qz, 52.65.Tt, 52.70.Gw

The understanding of turbulent fluctuations in the core of tokamak plasmas, causing a degradation of the confinement, is a crucial issue in view of future fusion reactors. Global empirical scaling laws based on the existing experiments [1,2] are often used to extrapolate the performance of the next generation devices like ITER and DEMO. However, predictive capabilities should rely on first principle models retaining comprehensive physics. Recently, relevant advances in magnetic fusion have been achieved through the validation of *ab initio* nonlinear numerical predictions of tokamak microturbulence [3,4]. In this Letter, nonlinear gyrokinetic simulations are quantitatively compared to turbulence measurements on the TORE SUPRA tokamak. The relevance of this analysis relies on the fact that the high-order scalar observables are coherently verified also through the investigation of the lower-order spectral quantities. With respect to the previous works, the present study is qualified by the simultaneous validation of (1) the total heat transport coefficient, (2) rms values of the density fluctuations δn, (3) k_θ, and (4) k_r wave-number δn spectra.

Analysis of the fluctuation spectral power density in the wave-number space transverse to the magnetic field (k_θ, k_r), poloidal and radial wave-vectors respectively, allows us to characterize the turbulence structure, and gives insight into its dynamics in terms of flow of the turbulent energy $E(k)$ at the scale $1/k$. On most experiments [5–7], the density fluctuation wave-number spectrum $S(k_\perp) = |\delta n(k_\perp)/n|^2$ shows a decay $S(k_\perp) \sim k_\perp^\alpha$ with $\alpha = -3.5 \pm 0.5$. The TORE SUPRA tokamak is particularly well suited to the study of local k spectra of density fluctuations in the medium-low range $k_\perp \rho_s < 2$ (where ρ_s is the ion-sound Larmor radius): it is equipped with complementary microwave diagnostics, fast-sweeping [8] and Doppler [9] reflectometers. Though the geometrical arrangement and measurement techniques are different, these two methods are both based on the detection of the field backscattered on density fluctuations, whose wave number matches the Bragg rule $k_f = -2k_i$, where k_i is the local probing wave vector. In the fast-sweeping system, the probing wave is launched in the equatorial plane, with a k_i in the radial direction. The fast sweeping of the probing frequency (from 50 to 110 GHz in 20 μs) allows sensitive measurements of the density profile $n(r)$. A high repetition rate (1 profile each 25 μs) is used to extract the density fluctuation profile $\delta n(r)$. The local k_r spectra can then be obtained using an iterative process of comparisons between full-wave simulations and experimental measurement [10]. The typical size of the spatial window allows probing the spectrum between $1 \lesssim k_r \lesssim 20$ cm^{-1}, with a resolution on the spatial localization of $\Delta r/a \approx 0.04$ (a is the plasma minor radius). Note that in this method, fluctuations with poloidal wave numbers up to $k_\theta \approx 10$ cm^{-1} are also included in the signal due to finite beam size. This has to be taken into account when comparing with theory or simulations. In the case of Doppler reflectometry system, the probing beam is launched in oblique incidence with respect to the cutoff layer. The scattering process is mostly localized at the cutoff, whose position is set by the (fixed) frequency of the beam [9]. In the case of O-mode beam polarization, the selected wave number is mainly poloidal and the rms value of the signal is directly proportional to the power spectrum of density fluctuations; the wave-number spectrum is then obtained by varying the antenna tilt angle. This allows us to probe the spatial domain $0.5 \lesssim r/a \lesssim 0.95$ and the range of wave numbers $4 \lesssim k_\theta \lesssim 15$ cm^{-1}, where only very small $k_r \lesssim 1$ cm^{-1} are included in the signal.

One standard TORE SUPRA L-mode Ohmic discharge has been chosen as target, TS39596, having toroidal field

TABLE I. Experimental parameters for the discharge TS39596; $\rho_* = \rho_s/a$, ν_{ei} frequencies are in units of c_s/a (c_s is the ion-sound speed) and s is the magnetic shear.

r/a	a/L_{T_i}	a/L_{T_e}	a/L_n	q	s	T_i/T_e	ρ_*	β	ν_{ei}
0.4	1.65	3.0	0.8	1.28	0.55	1.0	0.0023	0.42%	0.41
0.5	2.10	2.4	0.7	1.48	0.72	1.1	0.0020	0.31%	0.63
0.6	2.22	2.36	0.8	1.71	0.95	1.1	0.0018	0.22%	0.90
0.7	3.25	4.13	1.4	2.04	1.33	1.2	0.0016	0.17%	1.46

$B_T = 2.4$ T, plasma current $I_p = 0.8$ MA, central line density $n_{e0} = 4.5 \times 10^{19}$ m^{-2}, central electron temperature $T_{e0} = 1.1$ keV, and no external momentum input. Nonlinear simulations have been performed with the gyrokinetic Maxwell code GYRO [11] in the local (flux-tube) limit, using the experimental parameters summarized in Table I.

The electron-ion collisions are applied in the simulations through pitch-angle scattering. Electromagnetic effects are also retained, being β the ratio between kinetic and magnetic pressure. A realistic magnetic geometry via the Miller equilibrium model [12], is assumed for the circular cross section TORE SUPRA plasmas. The experimental effective charge Z_{eff} is 1.6, nevertheless, the simulations assume $Z_{\text{eff}} = 1$ and include gyrokinetic treatment of deuterium ions and drift-kinetic electrons with real mass ratio $\sqrt{m_i/m_e} = 60$. The simulations employ 128-point velocity space discretization (8 pitch angles, 8 energies, and 2 signs of velocity), a typical box size in the perpendicular plane $[L_x, L_y] = [122\rho_s, 122\rho_s]$ and a radial resolution such that $\Delta r/\rho_s = 0.33$. Simulations at $r/a = 0.7$ use 32 complex toroidal harmonics resolving $0.0 < k_\theta \rho_s < 1.59$ scales, while for $r/a = 0.4$, 0.5, and 0.6, the range $0.0 < k_\theta \rho_s < 1.0$ is solved with 20 Fourier modes. Statistical averages on the saturated nonlinear state are performed on a typical physical equivalent time of 2.6 ms.

The total effective heat diffusivity χ_{eff}, experimentally obtained from a power balance analysis performed with the CRONOS code [13], is defined as $\chi_{\text{eff}} = -(q_e + q_i)/[n(\nabla_r T_e + \nabla_r T_i)]$ where q_e and q_i are the electron and ion heat fluxes, respectively. The experimental uncertainty is estimated taking into account the time evolution of the profiles during 1 s. Making use of the relation $q_j = Q_j - 3/2 T_j \Gamma_j$, where Q_j and Γ_j are the energy and particle flux for a species j predicted by GYRO, a good agreement between the numerical expectations and the experimental profile of χ_{eff} within the error bars is achieved (Fig. 1). The exception of $r/a = 0.4$ is due to marginal turbulence found by the simulation on the experimental parameters. Nevertheless, the stiffness to $\nabla_r T_{i,e}$ (whose experimental uncertainty is about $\pm 30\%$) inherent in the transport problem [11], suggests that a reliable validation of the turbulence model cannot be limited to this scalar quantity.

The radial profile of the rms $\delta n/n$ measured by the fast-sweeping system is shown in Fig. 2. Consistently with the diagnostic, this quantity is calculated from the density fluctuations predicted by GYRO at the outboard midplane as $\delta n/n|_{\text{rms}} = (\int_{1\ \text{cm}^{-1}}^{10\ \text{cm}^{-1}} dk_r \int_{0\ \text{cm}^{-1}}^{10\ \text{cm}^{-1}} dk_\theta |\delta n/n(k_r, k_\theta)|^2)^{1/2}$. Figure 2 reports a quantitative agreement with the experimental radial profile within the error bars, matching also the slight increase of $\delta n/n$ towards external radii found by the diagnostic.

The density fluctuations k_θ spectrum at $r/a = 0.7$ from Doppler reflectometry is presented in Fig. 3. The present analysis focuses only on the region $k_\theta \rho_s \leq 1.0$, where a power law decay with spectral index $\alpha_\theta = -4.3 \pm 0.7$ is

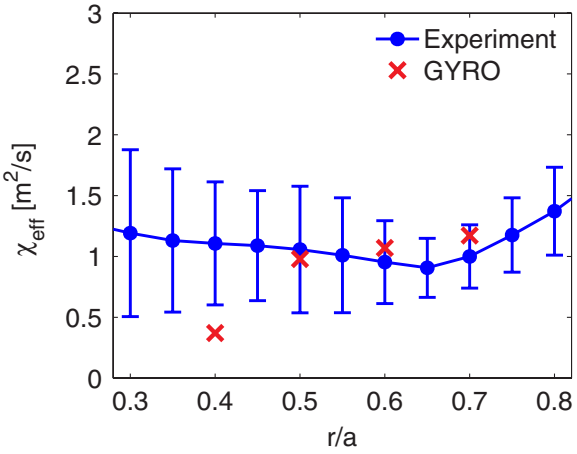

FIG. 1 (color online). Radial profile of the experimental effective heat diffusivity and comparison with the GYRO predictions.

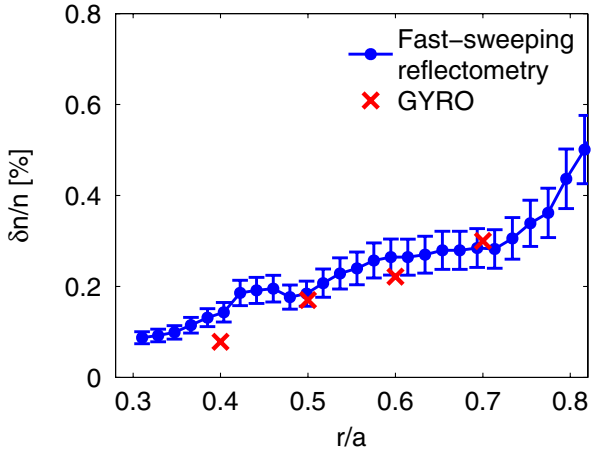

FIG. 2 (color online). Radial profile of the experimental rms $\delta n/n$ and comparison with the GYRO predictions.

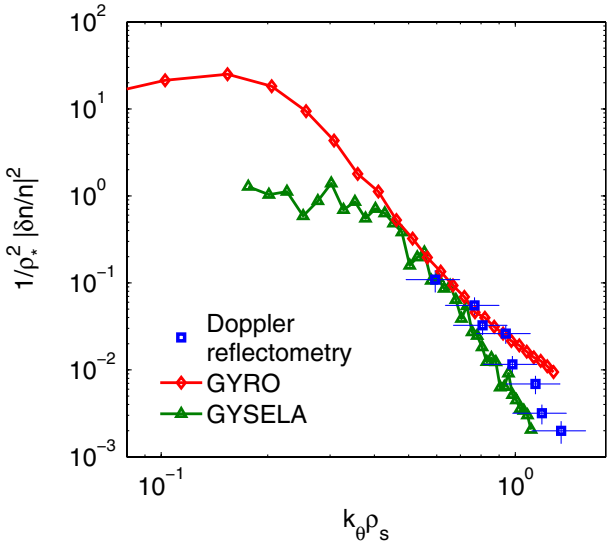

FIG. 3 (color online). Experimental density fluctuation k_θ spectrum at $r/a = 0.7$, and comparison with the GYRO and GYSELA predictions.

found. Eventual transition towards steeper slopes at $k_\theta \rho_s > 1$ as reported in Ref. [7] is not addressed here. To reproduce the Doppler measurements, the relation $S(k_\theta) = \int_{0\ \mathrm{cm}^{-1}}^{1\ \mathrm{cm}^{-1}} dk_r |\delta n/n(k_r, k_\theta)|^2$ is used on the δn simulated by GYRO at the outboard midplane. The simulation gives a spectral index of $\alpha_\theta = -4.3$ for $0.4 < k_\theta \rho_s < 1.0$, in remarkable agreement with the reflectometry data within experimental uncertainty. A similar agreement has also been recovered with global electrostatic simulations performed with the semi-Lagrangian gyrokinetic code GYSELA [14], where the equilibrium profile is self-consistently evolved. Long enough simulation runs allow the system to reach a new equilibrium, characterized by well defined averaged profiles which are controlled by both the prescribed temperatures at the radial boundaries and the turbulent transport level. The main additional difference with respect to GYRO simulations is the adiabatic assumption for the electron response, such that density and electrostatic potential fluctuations are equal. This approximation can be though justified in this case due to the high levels of collisionality. Local TORE SUPRA parameters have been matched in the global simulation at $r/a = 0.7$, but the normalized gyroradius was increased up to $\rho_* = 8 \cdot 10^{-3}$ because of limited numerical resources. However, that such a mismatch should not impact the results provided the turbulence exhibits a gyro-Bohm scaling, as expected at these low ρ_* values.

A full torus simulation on $0.5 < r/a < 0.9$ has been run with GYSELA using the grid points resolution $[r, \theta, \varphi, v_\parallel, \mu] = [256, 256, 128, 64, 8]$ (θ and φ are the poloidal and toroidal angles, $v_\parallel$ the parallel velocity, and μ the adiabatic invariant). GYRO makes use of the field-aligned coordinates $(r,\ \zeta = \varphi - q\theta,\ \eta = \theta)$, while GYSELA operate with the poloidal θ and toroidal φ angles. The following relationship between the Fourier components $\hat{\phi}_n^{\mathrm{GYRO}}(r, \eta) = \hat{\phi}_n^{\mathrm{GYSELA}}(r, \theta) \exp(inq\theta)$, with n the wave number along ζ or φ, allows one to compute the same spectra with the two different codes at $\theta = 0$. GYSELA k_θ fluctuation spectrum is also shown in Fig. 3, giving a spectral exponents $\alpha_\theta = -5.2$ for $0.4 < k_\theta \rho_s < 1.0$. In this global simulation, the spectral power density at low k_θ is flatter, likely due to the presence of large scale sheared flows in the frequency range of geodesic acoustic modes [15]. Their impact and dynamics will be addressed in a future publication. In the range $k_\theta \rho_s \geq 0.4$, the nonlinear cascades leads to spectra similar to the measured and the local GYRO ones. This evidence suggests that, in tokamak plasmas, the turbulence wave-number spectrum exhibits a rather general character, likely governed by the dominant nonlinearities in the system, namely, the $E \times B$ convection terms.

The local k_r density fluctuation spectrum from fast-sweeping reflectometry at the same radial position $r/a = 0.7$ is shown in Fig. 4. The measurements still exhibit a power law decay with a spectral exponent $\alpha_r = -2.7 \pm 0.25$ for scales corresponding to $0.4 < k_r \rho_s < 2.0$. This spectral quantity is reconstructed through the relation $S(k_r) = \int_{0\ \mathrm{cm}^{-1}}^{10\ \mathrm{cm}^{-1}} dk_\theta |\delta n/n(k_r, k_\theta)|^2$, which has been applied to the GYRO δn predictions at the outboard midplane. A very good agreement with the fast-sweeping reflectometry data is achieved, both in the magnitude and the slope of the relative fluctuation level, covering also the larger spatial scales up to $k_{r,\min} \approx 1\ \mathrm{cm}^{-1}$.

At the same radial location $r/a = 0.7$, the two reflectometers provide then different (above the experimental uncertainties) fluctuation spectral exponents in the perpen-

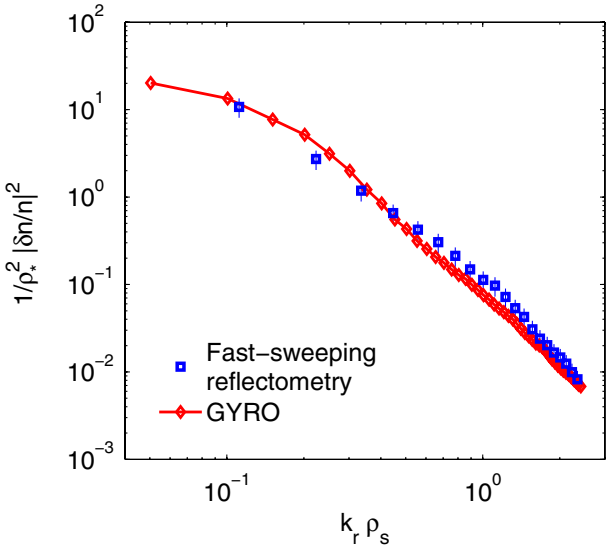

FIG. 4 (color online). Experimental density fluctuation k_r spectrum at $r/a = 0.7$, and comparison with the GYRO predictions.

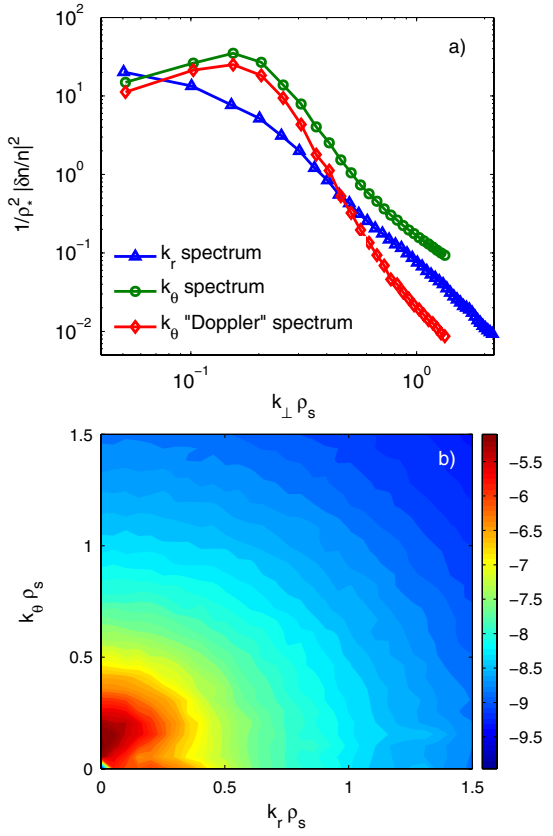

FIG. 5 (color online). (a) $|\delta n/n|^2$ spectra from the GYRO simulation at $r/a = 0.7$, and the impact of reconstructing the Doppler reflectometry instrumental response on the k_θ spectrum. (b) Contour plot of the GYRO $\log_{10}|\delta n(k_r, k_\theta)/n|^2$.

dicular plane, i.e., $\alpha_\theta = -4.3 \pm 0.7$ while $\alpha_r = -2.7 \pm 0.25$ for $k_\perp \rho_s \geq 0.4$ (Figs. 3 and 4). Such a discrepancy could suggest a highly anisotropic turbulence, favoring the formation of radially elongated structures. On the contrary, the GYRO results motivate a revised interpretation of this experimental evidence: the two dissimilar exponents may be simply ascribed to intrinsic instrumental effects. While for the fast-sweeping k_r spectrum the contributions of medium-low k_θ wave numbers are retained, the Doppler reflectometry k_θ spectrum selects only very low radial wave numbers [9]. The k_θ fluctuation spectral exponents predicted by GYRO clearly exhibit a difference when integrating over the Doppler range $0 < k_r < 1$ cm^{-1}, giving $\alpha_\theta = -4.3$ in agreement with the measurements, rather than $\alpha_\theta \approx -2.9$ when accounting for all the radial wave numbers [Fig. 5(a)]. A strong anisotropy carried by the peak in the k_θ axis significantly affects the $k_\perp \rho_s < 0.4$ ranges, while the asymmetry appears weaker, but still present, at smaller spatial scales [5,16]. The isolevel contours of $|\delta n/n(k_r, k_\theta)|^2$ in the perpendicular plane computed by GYRO [Fig. 5(b)] confirm the expected picture, identifying a linearly driven turbulence anisotropy around the $k_\perp \rho_s \approx 0.2$ scales, which are not accessible by our Doppler reflectometry.

In conclusion, nonlinear gyrokinetic GYRO simulations are here shown to quantitatively reproduce complementary measurements from a standard TORE SUPRA discharge, namely: heat χ_{eff}, rms $\delta n/n$, k_θ, and k_r spectra. When properly reconstructing the instrumental response, simulations help to revise the apparent experimental turbulence anisotropy at scales comparable to the ion gyroradius. Also, the similarity of the fluctuation k_θ power spectra between the measurements and both local and global gyrokinetic simulations, suggests a rather general character of the tokamak turbulence wave-number spectrum. Further analysis on the impact of the experimental uncertainties and different plasma scenarios on the simulation results (actually limited by the high computational cost), should assess the effectiveness of the nonlinear gyrokinetic codes in predicting the tokamak confinement properties.

The author would like to thank Dr. C. Holland for valuable discussions. This work, supported by the European Communities under the contract of Association between EURATOM, CEA, and the French Research Federation for fusion studies, was carried out within the framework of the European Fusion Development Agreement. Financial support was also received from the Agence Nationale de la Recherche ANR06-blan0084.

*alessandro.casati@cea.fr

[1] P. Yushmanov *et al.*, Nucl. Fusion **30**, 1999 (1990).
[2] S. M. Kaye *et al.*, Nucl. Fusion **37**, 1303 (1997).
[3] C. Holland *et al.*, J. Phys. Conf. Ser. **125**, 012043 (2008).
[4] L. Lin *et al.*, Phys. Plasmas **16**, 012502 (2009).
[5] C. P. Ritz *et al.*, Nucl. Fusion **27**, 1125 (1987).
[6] P. Devynck *et al.*, Plasma Phys. Controlled Fusion **35**, 63 (1993).
[7] P. Hennequin *et al.*, Plasma Phys. Controlled Fusion **46**, B121 (2004).
[8] F. Clairet *et al.*, Plasma Phys. Controlled Fusion **43**, 429 (2001).
[9] P. Hennequin *et al.*, Nucl. Fusion **46**, S771 (2006).
[10] T. Gerbaud *et al.*, Rev. Sci. Instrum. **77**, 10E928 (2006).
[11] J. Candy and R. E. Waltz, Phys. Rev. Lett. **91**, 045001 (2003).
[12] R. L. Miller *et al.*, Phys. Plasmas **5**, 973 (1998).
[13] V. Basiuk *et al.*, Nucl. Fusion **43**, 822 (2003).
[14] V. Grandgirard *et al.*, Plasma Phys. Controlled Fusion **49**, B173 (2007).
[15] K. Hallatschek and D. Biskamp, Phys. Rev. Lett. **86**, 1223 (2001).
[16] R. E. Waltz, J. Candy, and M. Fahey, Phys. Plasmas **14**, 056116 (2007).